Biochimica et Biophysica Acta 1864 (2016) 501–510

Contents lists available at ScienceDirect

Biochimica et Biophysica Acta

journal homepage: www.elsevier.com/locate/bbapap

Structural remodeling during amyloidogenesis of physiological N^{α}-acetylated α-synuclein

J. Ignacio Gallea [a], Rabia Sarroukh [b], Pablo Yunes-Quartino [a], Jean-Marie Ruysschaert [b], Vincent Raussens [b], M. Soledad Celej [a,*]

[a] Departamento de Química Biológica, Centro de Investigaciones en Química Biológica de Córdoba (CIQUIBIC, CONICET), Facultad de Ciencias Químicas, Universidad Nacional de Córdoba, Haya de la Torre y Medina Allende, Ciudad Universitaria, X5000HUA, Córdoba, Argentina

[b] Center for Structural Biology and Bioinformatics, Laboratory of Structure and Function of Biological Membranes, Faculty of Science, Université Libre de Bruxelles (ULB), Brussels B-1050, Belgium

ARTICLE INFO

Article history:
Received 20 November 2015
Received in revised form 25 January 2016
Accepted 27 January 2016
Available online 2 February 2016

Keywords:
Acetylated α-synuclein
Parkinson's disease
Fibrillation
Amyloid
Secondary structure
FTIR

ABSTRACT

The misfolding and aggregation of the presynaptic protein α-synuclein (AS) into amyloid fibrils is pathognomonic of Parkinson's disease, though the mechanism by which this structural conversion occurs is largely unknown. Soluble oligomeric species that accumulate as intermediates in the process of fibril formation are thought to be highly cytotoxic. Recent studies indicate that oligomer-to-fibril AS transition plays a key role in cell toxicity and progression of neurodegeneration. We previously demonstrated that a subgroup of oligomeric AS species are ordered assemblies possessing a well-defined pattern of intermolecular contacts which are arranged into a distinctive antiparallel β-sheet structure, as opposed to the parallel fibrillar fold. Recently, it was demonstrated that the physiological form of AS is N-terminally acetylated (Ac-AS). Here, we first showed that well-characterized conformational ensembles of Ac-AS, namely monomers, oligomers and fibrils, recapitulate many biophysical features of the nonacetylated protein, such as hydrodynamic, tinctorial, structural and membrane-leakage properties. Then, we relied on ATR-FTIR spectroscopy to explore the structural reorganization during Ac-AS fibrillogenesis. We found that antiparallel β-sheet transient intermediates are built-up at early stages of aggregation, which then evolve to parallel β-sheet fibrils through helix-rich/disordered species. The results are discussed in terms of regions of the protein that might participate in this structural rearrangement. Our work provides new insights into the complex conformational reorganization occurring during Ac-AS amyloid formation.

1. Introduction

The protein α-synuclein (AS) is highly expressed at the presynaptic termini of neurons. Its progressive accumulation and amyloid deposition in intraneuronal inclusions is pathognomonic of Parkinson's disease and other disorders, collectively called synucleinopathies [1]. Despite the large body of evidence supporting the key role of AS in the pathogenesis of these disorders, the molecular mechanisms underlying neurodegeneration and the exact nature of the toxic forms remain elusive [1]. A number of *in vitro* and *in vivo* studies demonstrate that soluble AS oligomers (oAS) that accumulate as intermediates during the process of fibril formation are highly cytotoxic [1,2]. In this regard, a variety of cellular dysfunctions has been assigned to oAS, including the imbalance of ion homeostasis, promiscuous binding to other proteins, mitochondrial damage, lysosomal leakage, and cell-to-cell transmission of the pathology [1,2]. Recent studies indicate that the oligomer-to-fibril AS conversion contributes to cell toxicity and progression of neurodegeneration, suggesting that this process itself, rather than just particular outcomes (*i.e.* oligomers or fibrils), plays a key role in cell fate [3–5].

Understanding the complex structural reorganization that takes place during oligomer and fibril formation is fundamental for shedding light into the molecular basis of AS-induced toxicity. Myriad conformational states are populated in the intermediate stages of aggregation, including partially folded intermediates and prefibrillar species varying in structure, size and morphology [6–11]. Although still limited, detailed studies on distinct aggregation ensembles have led to significant improvements in our knowledge of the structural characteristics of key players in AS fibrillation. In the insoluble amyloid form, the fibril core

Abbreviations: AS, α-synuclein; Ac-AS, acetylated α-synuclein; mAS, oAS, fAS, α-synuclein monomers, oligomers and fibrils respectively; mAc-AS, oAc-AS, fAc-AS, acetylated α-synuclein monomers, oligomers and fibrils respectively; NatB, N-terminal acetyltransferase B; IPTG, isopropyl-β-D-1-galactopyranoside; ThioT, Thioflavin T; 1,8-ANS, 1-anilino-naphthalene-8-sulfonate; POPG, 1-palmitoyl, 2-oleoyl phosphatidylglycerol; LUVs, large unilamellar vesicles; FPLC, fast protein liquid chromatography; SEC, size-exclusion chromatography; ESI-TOF-MS, electrospray ionization time-of-flight mass spectroscopy; TEM, transmission electron microscopy; ATR-FTIR, Attenuated total reflectance-Fourier transform infrared; IR, infrared; FSD, Fourier self-deconvolution; SD, second-derivative; FWHH, full width at half high; σ, standard deviation; ν, frequency; PPII, polyproline II; FRET, Förster resonance energy transfer; NMR, nuclear magnetic resonance.

* Corresponding author.
E-mail address: mcelej@mail.fcq.unc.edu.ar (M.S. Celej).

http://dx.doi.org/10.1016/j.bbapap.2016.01.011
1570-9639/

spans residues Glu[35]-Lys[96] from which the two termini are excluded [12]. The most accepted model of AS fibrils indicates that each molecule folds into a five-layered β-sandwich (β1 to β5) which then, through intermolecular interactions, forms the parallel in-register fibril [13]. In solution, AS is a natively unstructured monomer with transient secondary structures [14] and a complex network of long-range tertiary interactions among different regions of the protein, involving amino acids that are part of the β-strands forming the fibril core [15,16]. Interestingly, some of these pairwise interactions correlate with fibrillar contacts but others are mismatched with respect to those found in the amyloid fold [16]. On the other hand, oAS are structurally diverse. For instance, β-sheet-rich, largely disordered as well as primarily α-helical oligomeric species have been described ([17] and references therein). A number of studies on β-sheet-rich oAS indicate that they are ordered assemblies of distinct sizes, with a solvent-protected core spanning residues ~Phe[4]-Ala[90] and discrete stretches (Phe[4]-Ala[17], Tyr[39]-Thr[54] and Val[70]-Ala[89]) with hampered backbone dynamics [18,19]. It is recognized that β-sheets in the oligomeric and fibrillar states are different [20], likely due to a distinct antiparallel orientation of the β-strands in oAS, as opposed to the parallel orientation present in the amyloid fold [21–23]. Recently, we have proposed that segments corresponding to β1 (Val[37]-Lys[43]), β2 (Val[52]-Thr[59]) and β4 (Gly[68]-Val[77]) strands might be engaged in these early intermolecular antiparallel β-sheet interactions [24]. Hence, it is evident that AS amyloid formation demands an extensive structural reorganization of contacts throughout the aggregation pathway.

It has recently become clear that all detectable AS *in vivo*, both in physiological and pathological conditions, is N$^{\alpha}$-terminally acetylated (Ac-AS) [25]. It was demonstrated that this co-translational modification does not significantly affect the structure of the monomeric protein, its oligomerization state or localization in intact cells [26]. Several *in vitro* studies consistently showed that N-terminal acetylation of AS leads to a modest increase in helicity for the first ~10 residues, whereas its impact on lipid binding properties and aggregation rates has been more contradictory [26–29]. Taking into account that Ac-AS is the naturally occurring form of the protein, it is the characterization of its complex structural remodeling during amyloid formation that becomes fundamental to understand the role of oligomeric species and fibril formation in neurodegeneration and disease. Accordingly, in this work we relied on attenuated total reflectance-Fourier transform-infrared spectroscopy (ATR-FTIR) to gain insights into the structural transformation of Ac-AS during the entire process of amyloidogenesis. Our work highlights the complexity of the energy landscape leading to amyloid formation, providing direct evidence for the β-sheet remodeling that takes place at the level of prefibrillar species.

2. Materials and methods

2.1. Protein expression and purification

Ac-AS was expressed in BL21(D3) *Escherichia coli* cells co-transformed with a pT7-7 plasmid encoding for AS and a plasmid encoding for the N-terminal acetyltransferase B (NatB) [30]. The NatB plasmid was a kind gift from Dr. Daniel Mulvihill. Bacteria were cultured at 37 °C in LB medium with 25 μg/mL chloramphenicol and 100 μg/mL ampicillin. For the unmodified protein, *E. coli* cells transformed only with the plasmid encoding for AS were grown at 37 °C in LB medium containing 100 μg/mL ampicillin. Expression was induced by addition of 0.5 mM isopropyl-β-D-1-galactopyranoside (IPTG) once the cell culture had reached an OD_{600} of ~0.6. Cells were incubated afterwards at 37 °C for 4 h and harvested. Proteins were purified using a standard protocol that includes boiling and selective ammonium sulfate precipitation steps, followed by anion exchange chromatography, as previously described [21]. Protein concentrations were determined by absorbance ($\varepsilon^{275} = 5600\ M^{-1}\ cm^{-1}$).

2.2. Preparation of monomeric and aggregated species

Monomeric protein stock solutions (300 μM) were prepared in 25 mM Tris–HCl, pH 7.5 and filtered through Amicon Ultra-0.5 100 kDa cut-off filters (Millipore). For oligomer preparation, 300 μM protein samples were freeze-dried, redissolved in 25 mM Tris–HCl, pH 7.5 and centrifuged (20,000 × *g*, 30 min, 4 °C) to remove big particles. Oligomeric species were separated from the monomer using Amicon Ultra-0.5 100 kDa cut-off filters (Millipore). The procedure was repeated until tyrosine fluorescence emission detected in the flow-through was negligible as compared to the intensity measured in the retentate. The removal of the monomeric protein was confirmed by native gradient PAGE. The absence of amyloid fibrils was verified by Thioflavin T (ThioT) fluorescence. Fibrillation was achieved by incubating 300 μM monomeric protein solutions at 70 °C and shaking at 800 rpm, conditions that accelerate fibril formation [31]. Fibrils were isolated by consecutive cycles of centrifugation (14,000 × *g*, 30 min, 4 °C) and resuspension in 25 mM Tris–HCl, pH 7.5 buffer. For the aggregated species, protein concentration in monomeric units was determined by the absorbance of aliquots incubated in 6 M guanidinium chloride at 25 °C for 24 h.

2.3. Size-exclusion chromatography (SEC)

500 μL of monomeric protein solutions were loaded onto a Superdex 200 10/300 (GE Healthcare Life Sciences) column equilibrated with 25 mM Tris–HCl, pH 7.5 and eluted at 0.5 mL/min. The column was coupled to an AKTA FPLC system (GE Healthcare Life Sciences) equipped with a UV detector at 280 nm. A solution of bovine serum albumin (Sigma) at 8 mg/mL was used as a reference.

2.4. Native gradient PAGE

Native polyacrylamide gels were cast with a linear gradient from 4 to 15%. HMW native marker (GE Healthcare) was loaded as the molecular mass marker. Electrophoresis was performed under non-denaturing conditions at a constant 60 V and 4 °C. Gels were silver-stained.

2.5. Electrospray ionization time-of-flight mass spectroscopy (ESI-TOF-MS)

100 μM protein samples were 0.22 μm-filtered and supplemented with formic acid up to 0.1% prior direct injection into a ESI-Qq-TOF mass spectrometer, micrOQTOF-II (Bruker). Spectra were acquired from 250 to 2250 *m/z* in the positive ion mode using a capillary voltage of −5000 V and end plate offset of −500 V. The nebulizer pressure was 3.0 bar, whereas nitrogen flow was 7.0 L/min (as drying gas) at 180 °C. Mass calibration was achieved by injecting a sodium formate solution at 40 mM and selecting the best 8 signals according to the High Precision Calibration (HPC) fitting algorithm. An extra injection of calibrant after each protein sample was performed to increase precision. Protein solution injection rate was 10 μL/min. The software Data Analysis (Bruker) was used to process the data. Total ion chromatograms were averaged (2 min window). The averaged mass spectra were subjected to charge deconvolution after baseline subtraction and smoothing to obtain high resolution *m/z* data and charge status. Alternatively, data deconvolution was performed using the Maximum Entropy Algorithm to obtain neutral mass spectra. For both approaches, a theoretical mass restriction between 13,000 and 15,000 Da was employed, with proton adduct formation considered in the analysis.

2.6. Transmission electron microscopy (TEM)

5 μL of sample were adsorbed onto Formvar-coated carbon grids (200 mesh), washed with Milli-Q water and stained with 1% (*w/v*) uranyl acetate. The samples were imaged in a JEM-1200 Ex (Jeol) transmission electron microscope equipped with a GATAN camera, model 785.

2.7. ATR-FTIR

IR spectra of purified aggregated states were recorded on a Nexus IR spectrophotometer (Nicolet) and those during aggregation were acquired on an Equinox 55 IR spectrophotometer (Bruker Optics). Both instruments were equipped with a single reflection diamond reflectance accessory (Golden Gate, Specac) and purged with dry air to reduce water vapor distortions in the spectra. Aliquots of ~5 μL were dialyzed against water for 30 min to diminish buffer/salt concentration that distorts the IR protein profiles. Sample were spread on the diamond crystal, flushed with nitrogen and rehydrated using nitrogen saturated in ^2H_2O to obtain deuterated protein spectra. A total of 256 accumulations were recorded at 21 °C using a nominal resolution of 2 cm^{-1}. After subtraction of water vapor and side chain contributions, the spectra were baseline corrected and area normalized between 1600 and 1700 cm^{-1}. Spectra were processed and analyzed using Kinetics software (SFMB, Brussels, Belgium).

Identification of the overlapping bands, *i.e.* the number of underlying peaks within the amide I′ envelope, was carried out by Fourier transform self-deconvolution (FSD) and second-derivative (SD) analysis. FSD of the IR spectra before baseline subtraction was performed with a Lorentzian line (full width at half high FWHH = 30 cm^{-1}) and apodization with a Gaussian line (FWHH = 16.7 cm^{-1}) resulting in a line-narrowing enhancement factor K = 1.8. The position and number of the detected components were used as initial parameter for a least squares iterative curve fitting of the original (K = 1) IR spectra, using mixed Gaussian–Lorentzian band shapes. Fitting of the original spectra avoids artifacts due to band-resolution enhancement methods. An additional band at the low-wavenumber edge of the amide I′ region was introduced to improve the fittings. The positions and FWHH values of each individual component were constrained within physically plausible ranges expected for each type of secondary structure [32–35], which were assigned according to experimental reported data [33,34,36]. The position constrains given in cm^{-1} were 1696–1686 (β-sheet high-wavenumber component), 1628–1620 (β-sheet low-wavenumber component), 1660–1640 (helix/random) and 1680–1668 (turn). FWHH initial values in cm^{-1} were 9 (β-sheet high-wavenumber component), 17 (β-sheet low-wavenumber component), 43 (helix/random) and 20 (turn), varying between 8 and 11, 14 and 19, 30 and 56, and 5 and 30, respectively.

2.8. Fluorescence measurements

Emission spectra of purified aggregated states were acquired on a Cary Eclipse spectrofluorimeter (Agilent Technologies) equipped with a thermally controlled multi-cuvette holder. Ten spectra were recorded at 25 °C in a 1.5 mm path cuvette and averaged. 1-Anilino-naphthalene-8-sulfonate (1,8-ANS) emission spectra were obtained after 30 min incubation at room temperature of mixtures containing 5 μM protein and 100 μM dye in 25 mM Tris–HCl, pH 7.5. 1,8-ANS was excited at 370 nm, with excitation/emission slit widths of 10/10 nm. For dye release determinations, carboxyfluorescein was excited at 492 nm, with excitation/emission slit widths of 5/5 nm. ThioT measurements were performed at final concentrations of 0.5 μM protein and 5 μM dye in 50 mM glycine buffer, pH 8.2, using λ_{exc} = 446 nm, spectral bandwidths of 10 nm and a 1 cm path cuvette at 25 °C. ThioT fluorescence during aggregation was recorded on a LS55 spectrofluorimeter (PerkinElmer Instruments) equipped with a thermally controlled multi-cuvette holder.

2.9. Protein aggregation assay

The assembly reactions were carried out at 100 μM protein concentration in 25 mM Tris–HCl, pH 7.5, 100 mM NaCl, and 0.01% Na-azide at 37 °C under continuous stirring (350 rpm) according to standard procedures [21,31]. Samples were withdrawn at different time points during aggregation and assayed for amyloid formation (ThioT measurements) and structural transitions (ATR-FTIR measurements). Samples were run at least in triplicates and analyzed independently. Kinetic traces of amyloid formation were analyzed according to the equation $y = 1/\{1 + \exp[-k_{app}(t - t_{1/2})]\}$, where k_{app} is the apparent rate constant for the incorporation of monomers at the growth points, $t_{1/2}$ is the half-time of apparent amyloid conversion and the lag time is defined as $t_{1/2} - 2/k_{app}$ [7].

2.10. Dye leakage assay

1-Palmitoyl, 2-oleoyl phosphatidylglycerol (POPG) was obtained from Avanti. Large unilamellar vesicles (LUVs) were prepared by extrusion [37]. POPG dissolved in chloroform/methanol (2:1, *v*/*v*) was dried under gentle stream of N_2 onto the wall of a glass tube, and then placed in vacuum for 1 h to remove any remaining solvent. The lipid film was then rehydrated in 10 mM HEPES, 50 mM NaCl, 1 mM EDTA, and 50 mM 5(6)-Carboxifluorescein, pH 7.5 buffer. The sample was vortexed for 5 min and then extruded 20 times through polycarbonate membranes (100 nm pore diameter) at 25 °C. Nonencapsulated dye was removed by gel filtration through a Sephadex G-25, PD-10 column (General Electric) equilibrated with 10 mM HEPES, 150 mM NaCl, and 1 mM EDTA, pH 7.5 buffer. Vesicle diameter was 103 ± 36 nm according to dynamic light scattering measurement on a Nicomp 380 instrument (Particle Sizing Systems). Final lipid concentration was determined by organic phosphate quantification [38]. LUVs (20 μM) and the distinct aggregated protein species (1 μM) were incubated for 30 min at room temperature and assayed for 5(6)-Carboxyfluorescein release. Following background subtraction, leakage was expressed as a percentage of the maximum signal reached after vesicle disruption induced by the addition of 0.1% (*w*/*v*) Triton X-100. The experiments were performed in triplicates.

3. Results

3.1. General properties of distinct Ac-AS conformational ensembles

A major aim of our investigations has been to define the structural and biological features of key conformational ensembles of AS, namely monomers, oligomers and fibrils (mAS, oAS and fAS, respectively) [21,24,39]. However, a detailed biophysical characterization of the distinct conformational ensembles of the physiologically relevant Ac-AS is still missing. Therefore, before exploring the structural reorganization during amyloidogenesis of Ac-AS, we used a range of complementary biophysical techniques to define the specific features of monomers, oligomers and fibrils of the acetylated protein (mAc-AS, oAc-AS and fAc-AS, respectively).

We produced Ac-AS taking advantage of a recombinant protein co-expression strategy recently developed to obtain N-terminally acetylated eukaryotic proteins [30]. The protein was purified using a standard purification protocol which includes boiling and salting out steps. The resulting purified protein was analyzed by ESI-TOF-MS. After charge deconvolution, the main peaks were consistent with a molecular mass of 14,502 Da (expected mass 14,502.1 Da), in accordance with the addition of a single acetyl group (Fig. 1a, upper panel). Besides, MS confirms an efficiency of acetylation close to 100% since no unmodified protein (molecular mass 14,460 Da) was observed in the Ac-AS sample (Fig. 1b). The recombinant acetylated protein eluted as a single peak at 13.5 mL using analytical gel-filtration chromatography (Fig. 1c). The fact that the protein behaves hydrodynamically as a much larger protein when compared with a globular protein standard is consistent with its monomeric unfolded state [26,27].

We then employed the same protocols previously used to generate aggregated species of AS [21,24,39], to produce oAc-AS and fAc-AS. Briefly, we used lyophilization, an approach widely used to increase the formation of oligomeric species [18,22,23], to generate an ensemble of oligomeric species in a short time frame and at the required yields for

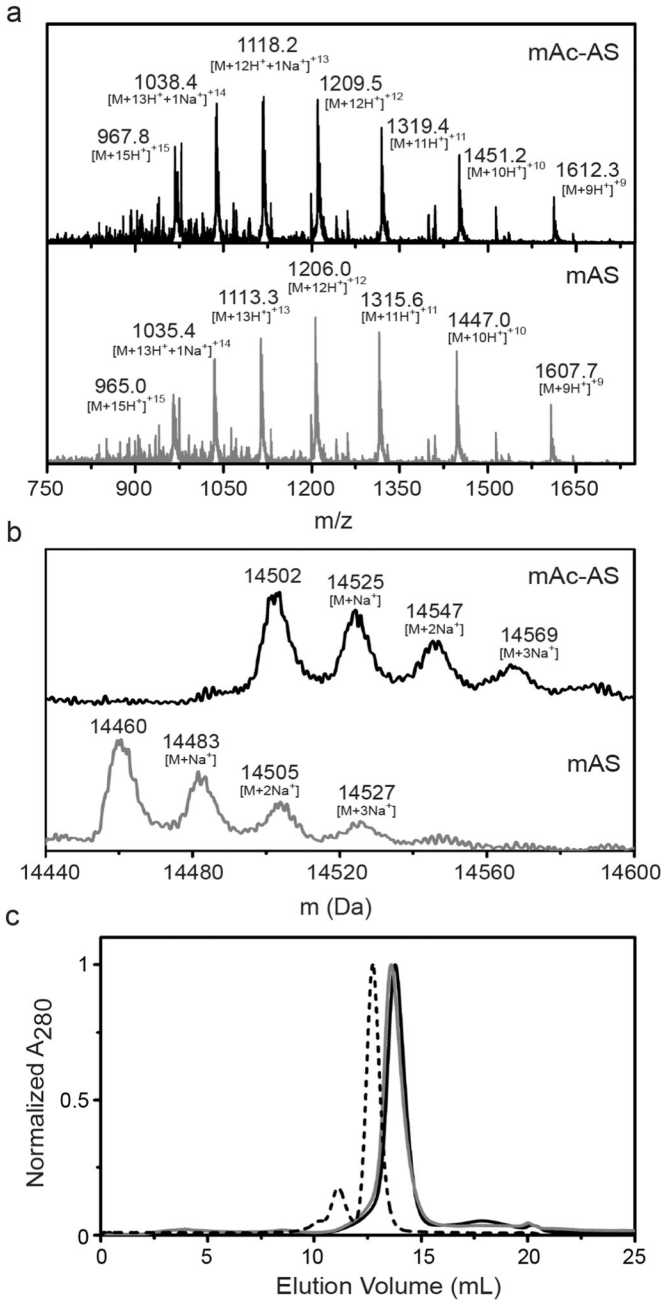

Fig. 1. Identification of *in vitro* AS acetylation. (a) Characterization of recombinant mAc-AS (▬) sample by ESI-TOF-MS. mAS sample is shown as a control (▬). Peaks are labeled with the charge state $[M + xH^+]^{x+}$, where M denotes the molecular mass of the protein. Molecular masses were calculated from the predominant *m/z* peak envelopes giving an observed mass of 14,502 Da and 14,460 Da for the acetylated and the unmodified protein, respectively. (b) Neutral mass spectra of both samples obtained by data deconvolution using the Maximum Entropy Algorithm. Sodium adducts are indicated. Line code as in panel a. (c) Analytical gel filtration profile of purified recombinant mAc-AS (▬). mAS (▬) and BSA (▬ ▬) were used as references.

in vitro studies [21,24,39]. On the other hand, fibrils were formed at high temperature with shaking, conditions that lead to faster aggregation kinetics [31].

We first analyzed the dispersity and morphology of the three conformational ensembles. Consistent with SEC experiments, mAc-AS migrated at an apparent molecular mass slightly above 66 kDa on a native gradient gel (Fig. 2a) and displayed electron micrographs devoid of nano-sized aggregates (Fig. 2b, left panel). oAc-AS ran as a smeared band in a native gradient PAGE, migrating near the molecular mass marker of ~440 kDa (Fig. 2a), indicating that they contain a distribution of particle sizes but not monomeric protein. These purified oligomeric species appeared as polydisperse spherical-like aggregates in TEM images (Fig. 2b, middle panel), with diameters ranging between 20 and 60 nm. fAc-AS were unbranched, several micrometers in length, with widths of 9–14 nm (Fig. 2b, right panel).

Then, we characterized structural features of the three conformational ensembles by means of fluorescence spectroscopy. ThioT is an amyloid-specific probe that exhibits significant changes in fluorescence upon intercalation into the cross-β fibrillar core [40]. At equivalent mass concentrations, fAc-AS displayed 10 times more ThioT fluorescence than mAc-AS or oAc-AS (Fig. 2c). These data suggest that the nature of the β-sheet structure present in oligomeric and fibrillar species of Ac-AS is different, correlating with previous reports on AS [20–23]. In addition, we used the solvatochromic dye 1,8-ANS to assess the extent of accessible hydrophobic patches in each species. The steady-state emission of the probe in the presence of the monomeric protein was low, with a maximum around 515 nm, much alike the fluorescence of the dye in buffer alone (Fig. 2d), indicating that it either interacts poorly with the monomers or that it is bound in a solvent-exposed mode [31]. Similarly to other ANS derivatives, the weak fluorescence signal of 1,8-ANS in the presence of the native protein may arise from electrostatic interactions between the anionic form of the dye and positively charged residues of the proteins and/or hydrophobic interactions between the naphthalene moiety of the probe with transient highly-solvent-exposed hydrophobic surfaces on the disordered monomer [31]. Upon mixing with the aggregated forms, there was an enhancement of fluorescence intensity (about twofold in fibrils and fourfold in oligomers), along with a blue-shift of ~35 nm (Fig. 2d), in agreement with previous reports on the nonacetylated protein [23]. These changes suggest that the bound dye experiences a hydrophobic microenvironment in the aggregated forms, being slightly greater in the oligomers.

Next, we tested the ability of the distinct protein species to disrupt synthetic membrane vesicles. For this purpose, 50 mM carboxifluorescein was entrapped inside POPG LUVs, a concentration at which dye fluorescence is self-quenched. Upon dye release from the vesicle, fluorescence intensity is dramatically enhanced. The extent of dye leakage from the liposomes was clearly dependent on the protein aggregation state. At equivalent mass concentration, mAc-AS and fAc-AS were able to disrupt the LUVs, but oAc-AS were the most effective in perturbing membrane permeability (Fig. 2e). Besides, based on reported data [41], we conclude that leakage ability does not depend on the nature of the protein since acetylated and non-acetylated forms follow similar trends.

Finally, deeper details about the secondary structure of the purified conformational states were gathered from ATR-FTIR, a technique widely used to study protein structure [34–36] and especially suitable for amyloid aggregates [42,43]. The so-called amide I′ band, located between 1700 and 1600 cm^{-1}, represents predominantly the amide C═O stretching. Since the precise frequency of the vibrations depends on the relative orientations, distances and phases of the coupled oscillating dipoles of neighboring amide groups, the amide I' band turns sensitive to protein secondary structure [33,34,36]. In addition, IR spectroscopy has proven valuable to distinguish between antiparallel and parallel β-sheets since the former presents a large splitting of the amide I' signal displaying a major absorption band at ~1630 cm^{-1} and an additional ~5-fold weaker band *circa* 1695 cm^{-1}, whereas the latter only presents the low-frequency band component [32,35,36,44]. Enhancement methods, such as derivation and deconvolution, allow the resolution of the protein spectra contour into overlapping components arising from the distinct structural elements. We resolved the amide I′ region using SD and FSD followed by curve-fitting of the non-deconvoluted IR spectra while constraining some of the fitting parameters within physically plausible ranges (see Section 2.7 for details). Although the accuracy of the determination of secondary structure composition is subject to some uncertainty arising from curve-fitting routings, it provides useful information about relative changes. The absorption and FSD

spectra of representative samples along with the fitted bands are shown in Fig. 2f. The band fitting analysis and assignments are summarized in Table 1.

The amide I′ band of mAc-AS was centered at ~1643 cm^{-1}, as expected for a substantially disordered protein (Fig. 2f, left panel). This result is in agreement with previous reports demonstrating that N^{α}-acetylation does not alter significantly the native unfolded conformation of the protein even if it induces an increase in helicity in the first ~10 residues [26–28]. The band positioned at 1642 cm^{-1} accounting for ~65% of the total amide I' absorption is assigned to disordered structure (Fig. 2f and Table 1). This broad band however might reveal some helical contribution (observed absorbances 1640–1660 cm^{-1} in deuterated conditions depending on the geometry, symmetry or interactions [34]), which we were unable to unambiguously resolve in the amide envelope. The absorption at 1622 cm^{-1} (~15% of the absorption), traditionally assigned to β-sheet structures, could also contain contributions from polyproline II (PPII) conformations [45,46]. The presence of PPII secondary structures in AS has been previously suggested by other optical techniques [47–49]. More recently, solution NMR-based methods have demonstrated that the PPII region is sampled within the conformational ensemble of the monomeric protein [50–52]. On the other hand, the IR spectrum of oAc-AS indicated an enhanced β-sheet structure as judged by a better resolved band at ~1620 cm^{-1} (Fig. 2f, middle panel and Table 1). This band appeared concomitantly to a weak but significant shoulder at 1694 cm^{-1}, more easily visualized in the FSD spectra shown as dot lines in Fig. 2f. The concomitant appearance of these two bands suggest an antiparallel orientation of the β-strands [32,35,36], the distinctive structural signature we previously proposed for oAS ([21]). The FTIR profiles also indicated a significant contribution from α-helix/disordered structures (Fig. 2f, middle panel), somehow increased in the oligomeric populations (Table 1). Far-UV CD studies on AS oligomeric species prepared by comparable methods have consistently showed that they contain β-sheet structures [22,23,53], likely in combination with disordered conformations as judged by the absence of the characteristic double minima of α-helix in their CD spectra. In line with this interpretation, antiparallel β-sheet oligomers with an outer rim of flexible proteins [22] or a hollow cylindrical architecture with a high degree of disorder [23] were described. On the other hand, helix-rich intermediates populated at early stages of AS aggregation under certain experimental conditions were reported [9,10]. As compared with the monomeric protein, we observed a shift of the helix/random component towards higher wavenumbers which could be reflecting an increment of spectroscopically unresolved helical contributions (Fig. 2f and Table 1). Lastly, the IR profile of fAc-AS displayed a prominent maxima at ~1625 cm^{-1} (Fig. 2f, right panel), a spectral region characterizing β-sheets in amyloid fibrils [42]. The absence of the high frequency peak indicates a parallel β-strand arrangement [35,36,44], as reported for the amyloid fold of the unmodified protein [13].

Overall, we established that distinct Ac-AS conformational ensembles are remarkably similar, in terms of hydrodynamic, morphological, tinctorial, structural, and membrane-leakage properties, to those

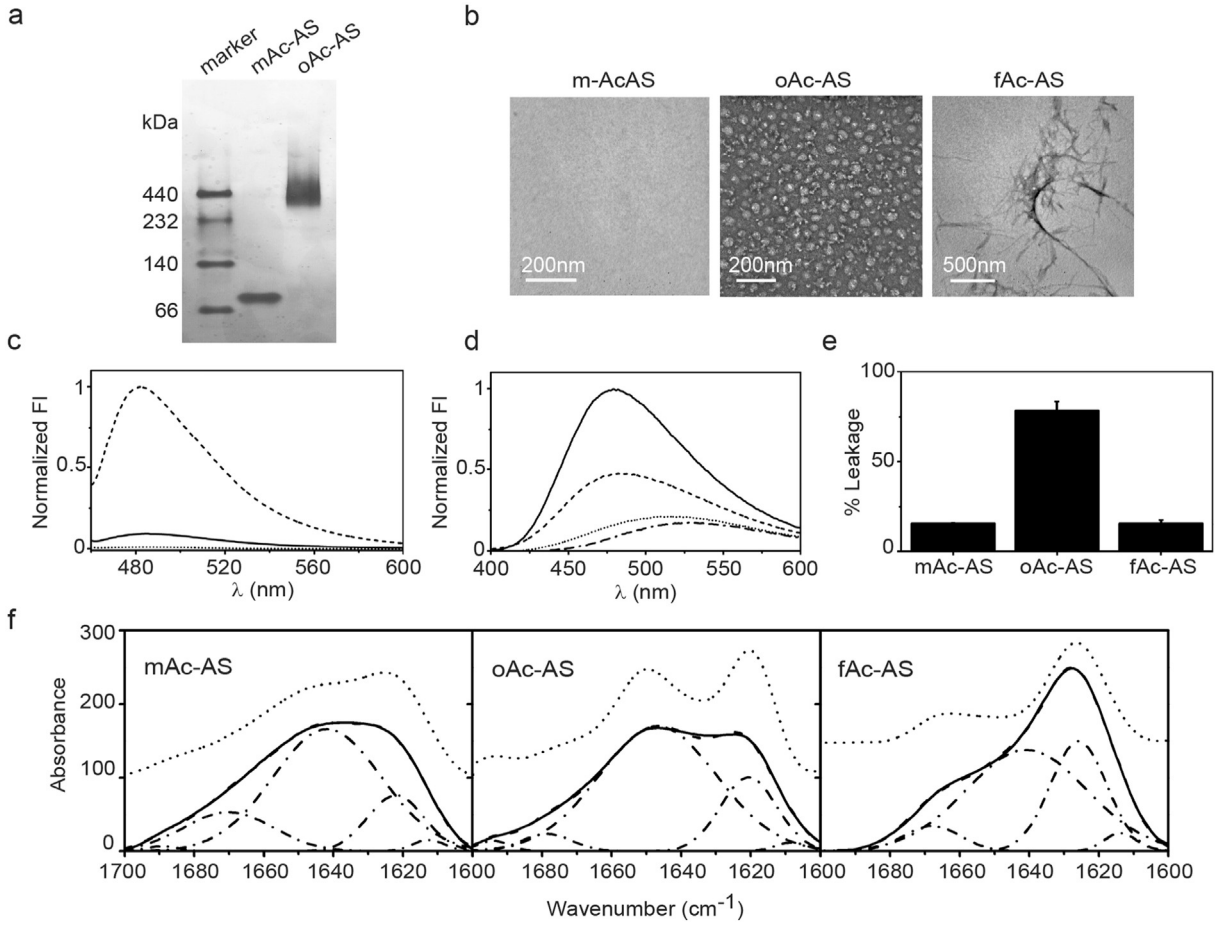

Fig. 2. General properties of Ac-AS conformational ensembles. (a) Native gradient PAGE with a polyacrylamide gradient from 4 to 15% stained with silver nitrate. (b) Uranyl acetate-stained transmission electron microscopy images of the three distinct Ac-AS species. (c) Normalized ThioT fluorescence emission spectra and (d) normalized ANS fluorescence emission spectra in the presence of mAc-AS (▪▪▪), oAc-AS (▬), fAc-AS (▬ ▬) or buffer alone (▬▪▬). (e) 5(6)-Carboxyfluorescein release from POPG LUVs in the presence of distinct Ac-AS species. Data in panel e are mean values ± standard deviation (σ) of three independent experiments. (f) Area-normalized FTIR absorbance spectra (▬) in the amide I′ region of isolated Ac-AS conformational ensembles. The spectra were curve fitted using five spectral components (▬▪▬). The Fourier self-deconvoluted spectra (▪▪▪) with a resolution enhancement factor K = 1.8 are also included in each panel and shifted for better visualization.

generated from the nonacetylated protein. More importantly, we conclude that membrane-disrupting oAc-AS possess a distinctive antiparallel β-sheet structure in combination with helical and disordered structures and exhibit a high degree of accessible hydrophobic patches.

3.2. Build-up of early antiparallel β-sheet intermediates during amyloidogenesis of Ac-AS

After establishing that a purified oAc-AS ensemble is arranged in antiparallel β-sheets, we aimed at determining whether this structural feature is present in pre-fibrillar intermediates transiently populated along amyloidogenesis. The kinetics of amyloid formation is consistent with a nucleation–polymerization mechanism, consisting of an initial lag-phase where nucleation centers spawn oligomeric species that lead to an exponential elongation phase and end in the formation of mature amyloid fibrils in the stationary phase. To study the structural evolution throughout the entire pathway of protein aggregation, we employed time-dependent ATR-FTIR spectroscopy to monitor structural transitions and ThioT fluorescence to assess the kinetics of amyloid formation.

Fig. 3a shows the FSD-IR profiles in the amide I′ region at different time points, qualitatively representing the structural evolution taking place during aggregation. Within the first 9 h of Ac-AS aggregation, the IR profiles displayed the concomitant appearance of the high and low-frequency components of antiparallel β-sheets (Fig. 3a). Interestingly, at 12 h these two bands drastically decreased and the amide envelope became almost flat in the 1650–1620 cm^{-1} region, with a maximum at ~1645 cm^{-1} indicative of a majority of helical/unordered structures. As aggregation proceeded, a pronounced peak located at ~1627 cm^{-1} was clearly observed. This, along with the absence of a second peak at higher wavenumbers (~1695 cm^{-1}) is attributed to the β-sheet parallel conformation of protofilaments and mature fibrils.

From the FSD spectra, we then calculated the so-called β-sheet organizational index (β-index for short), defined as the ratio between the high and low wavenumber β-sheet components, to monitor the time-reorganization of the β-strands [43]. The β-index profile along with the normalized kinetic aggregation curve measured by ThioT are depicted in Fig. 3b, upper panel. Ac-AS aggregation exhibited the classical sigmoidal aggregation profile expected for a nucleation–polymerization mechanism. Analysis of the kinetic ThioT curve indicated that Ac-AS forms fibrils with a lag-time of 12 h, an aggregation $t_{1/2}$ ~ 23 h, and an apparent growth rate constant k_{app} ~ 0.17 h^{-1}, in agreement with previous observations [28]. This monomer-to-fibril transition was accompanied by an initial increase of the β-index during the lag-phase and a subsequent decrease at longer times, evidencing the build-up and further disappearance of early β-sheet antiparallel species. A previous FTIR aggregation study performed on a FRET-AS variant, also showed the formation of transient β-sheet rich oligomers during the lag-phase [8], although no indication of the spatial arrangement of the β-strands was given.

We then performed a quantitative analysis of the amide I' band along the self-assembly process in order to get a better understanding of the structural reorganization during amyloidogenesis. The results after curve-fitting are included in Fig. 3b. Soon after the start of the aggregation, the total β-sheet content raised (Fig. 3b, lower panel) with a noticeable contribution of the high-wavenumber β-sheet component (Fig. 3b, upper panel), denoting the formation of antiparallel β-sheet rich species at early stages of amyloid formation. At the outset of the elongation phase, the total β-sheet content as well as the contribution of the high frequency β-sheet component diminished, and the α-helix/random contribution increased concomitantly (Fig. 3). The appearance of helix-rich intermediates at the onset of fibril growth and up to the mid-elongation phase has been recently revealed in a number of AS-related variants [10], in line with our observation. At the midpoint of the aggregation, the β-sheet contribution was about 2.5 greater than that at the beginning of the growing phase (from ~9% up to ~25%), and it increased a further 25% at the end of the stationary phase. This contribution mainly arose from the low-wavenumber β-sheet components corresponding to β-strands arranged in a parallel conformation directly showing the remodeling of the β-structure (Fig. 3). This increase paralleled the change in ThioT fluorescence sensing the cross-β fibrillar structure. The gain in β-sheet content was accompanied by a concomitant drop in helical/random contribution from ~70% to ~55%, whereas the turn content remained near 15% throughout the process (Fig. 3b).

Our IR study directly demonstrates that the substantial structural reorganization that takes place in the monomer-to-fibril transition of Ac-AS, demands a change in the spatial orientation of the β-structures at the level of prefibrillar intermediates.

Table 1
Secondary structure analysis of distinct Ac-AS species assessed by FTIR[a].

	mAc-AS		oAc-AS		fAc-AS	
Band assignment	ν (cm^{-1})	% area	ν (cm^{-1})	% area	ν (cm^{-1})	% area
β-Sheet	1689	0.8	1694	1.7	–	–
	1622	15.4	1621	20.4	1626	30.3
	1613	1.8	1608	1.4	1614	2.8
Random/α-helix	1642	65.1	1647	72.3	1641	60.0
Turn	1670	16.9	1679	4.2	1668	6.9

[a] Mean values of three independent experiments. $\sigma\,\nu \pm 1$ cm^{-1}; area ± 0.1–2.0%.

4. Discussion

Self-assembly of polypeptides into amyloid fibrils is usually detrimental for cells and it is associated to a number of pathological conditions. Nowadays, special attention is given to prefibrillar amyloid intermediates since they are presumed to be highly cytotoxic [1,54]. Major efforts in a number of laboratories have been directed at investigating the conformations of aggregation-prone species, the conformational changes occurring along the fibrillation pathway and the structural basis governing amyloid-induced toxicity. We have directed our efforts to provide fundamental knowledge into the internal architecture of amyloid oligomers of AS, a protein related to Parkinson's disease and other neurodegenerative maladies [1]. Similar to other amyloidogenic proteins, these species exist in a range of sizes, structures and inherent toxicities. Structurally, oAS have been classified in three broad classes: β-sheet-rich, largely disordered and primarily α-helical ([17] and references therein). In previous works, we overcame technical difficulties arising from the transient and heterogeneous nature of fibrillar intermediates and produced an ensemble of kinetically stable microstates of oAS which allowed us to study its structural and immunological attributes [21,24,39]. We showed that these oAS are likely to consist of antiparallel β-sheets with a defined pattern of intermolecular interactions [21,24]. In particular, we postulated that fibril-like β1–β1, β2–β2 and β4–β4 contacts (stretches Val^{37}-Lys^{43}, Val^{52}-Thr^{59} and Gly^{68}-Val^{77}, respectively) might be engaged in oligomeric antiparallel β-sheet interactions [24]. The adoption of such distinct β-sheet geometry has been recently linked to the thermodynamic and kinetic stability of this type of oligomeric species [23]. Taken together a number of studies reporting on the conformational properties of the monomeric [14–16,26–28], oligomeric [20–24] and fibrillar [12,13,55] ensembles, it emerges that a rearrangement of β-strand contacts is required for AS amyloid formation. Hence, we relied on ATR-FTIR to reveal the β-sheet remodeling on the physiologically relevant N^{α}-acetylated form of AS, Ac-AS.

Although N-terminal acetylation is one of the most abundant modifications of eukaryotic proteins, its biological function is still poorly understood. It has recently become clear that *in vivo* AS in human cells is subject to N^{α}-acetylation [25]. In this regard, there is a general consensus that the addition of the acetyl group slightly increases helicity of the N-terminal region of the monomeric protein [26–28]. However, contradictory results have been reported concerning the role of AS N-terminal

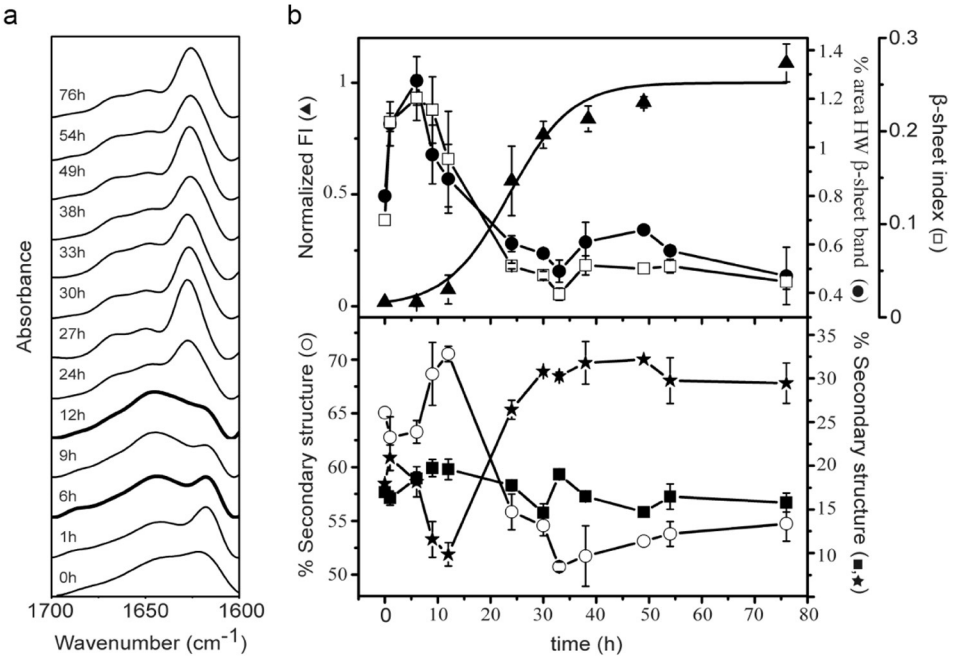

Fig. 3. β-Sheet remodeling and structural changes throughout the amyloidogenesis of Ac-AS. (a) Fourier self-deconvoluted FTIR spectra in the amide I′ region with a resolution enhancement factor K = 1.8 of Ac-AS at different specified times of the aggregation kinetic. (b) Kinetics of amyloid formation monitored by ThioT fluorescence (▲) along with the progression of the β-index (□) and the percentage of the high-wavenumber β-sheet band area (●), upper panel, and evolution of the content of β-sheet (★), α-helix/random coil (○) and β-turn (■) structures, lower panel. Spectral components were resolved after curve fitting of the K = 1 FTIR spectra. Each point represents the mean ± σ of three independent experiments.

acetylation on membrane/subcellular localization [26,56], vesicle binding [26,27] and aggregation propensity [26,28,29]. In this work, we showed for the first time that N^{α}-acetylation does not have a prominent effect on the biophysical properties of distinct conformational ensembles of the protein (Fig. 2). The immediate practical consequence of this finding is that one can extrapolate all the knowledge gathered over the years regarding the biophysical properties using recombinant AS to a system that better mimics the natural state of the protein *in vivo*. Future work needs to be done to resolve the discrepancies and elucidate whether AS N^{α}-acetylation regulates physiological and/or pathological processes. One possibility of such modification could be related to the Ac/N-end rule pathway which, as part of the ubiquitin system, participates in the regulation of the *in vivo* half-life of proteins [57].

We demonstrated that oAc-AS exhibited the FTIR spectral signatures attributable to antiparallel β-sheet structure, substantial amounts of helical/random structures and a high extent of accessible hydrophobic surfaces (Fig. 2 and Table 1). In line with these findings, we note that a variety of subgroups of oAS generated using comparable experimental approaches, although differing in their apparent morphologies, exhibit a substantial hydrophobic character and possess antiparallel β-sheet structures in combination with a large proportion of disordered structures [21–23]. In addition, these isolated oligomeric ensembles produced from lyophilized protein stock solutions resemble the so-called "fuzzy balls" reported by Jovin and co-workers, nanospheres detected at early stages of AS aggregation that exhibit a tendency to recruit material at their peripheries [11].

On the other hand, the FTIR data also suggest an increment of the helical contribution relative to the random structure in oAc-AS as compared to the monomeric protein (Table 1). The N-terminal region of the protein (residues 1–60) contains degenerated 11-residue repeats typical of amphipathic α-helical lipid-domains of apolipoproteins [58] and indeed adopts an α-helix conformation upon binding to acidic vesicles [14]. It has been shown that the core of AS spans residues ~Phe^{4}-Ala^{90} [18], where discrete specific stretches of amino acids exhibit hampered backbone dynamics reflecting the presence of stable hydrogen-bonded structures [19]. Strikingly, the segment encompassing residues Phe^{4}-Ala^{17} is protected against isotopic exchange indicating a structuring of the distal N-terminal region [19]. In line with these findings, we previously showed that pyrene-labeled oAS exhibit high excimer signals at selected positions within the N-terminal portion denoting a tight packing and a specific intermolecular contact network, speaking in favor of the acquisition of a regular structure in this region [24]. Therefore, we postulate that the increased helical contribution in oAc-AS would be mediated by the structuring of the N-terminal portion of the protein, highlighting the importance of this region on early oligomeric interactions. Overall, it appears that this oligomeric ensemble is organized in antiparallel β-sheets (likely engaging intermolecular β1–β1, β2–β2 and β4–β4 contacts [24]), in combination with helical (probably involving the N-terminal region) and disordered structures, and exposed hydrophobic patches.

Along the course of Ac-AS aggregation, the spectroscopic signals reporting on antiparallel β-sheet structure (β-index and low-wavenumber β-sheet component) rouse, peaked and then diminished before the maximal ThioT response, revealing the build-up and further consumption of early intermediates, in which protein molecules adopt a β-sheet geometry distinguishable from that acquired in the final fibrillar product (Fig. 3). Interestingly, this difference in β-sheet organization, from an antiparallel geometry in intermediates species to a parallel one in the fibrillar form, has been reported previously for other amyloidogenic proteins such as Aβ peptides [59,60], a prion-related peptide [61], β2-microglobuline [62], lysozyme [63] and the Josephin domain of ataxin-3 [64]. We have previously suggested that such β-sheet organization might represent a common structural motif in amyloid oligomers underlying their common membrane-disrupting pathogenic actions [21,59,60]. The antiparallel-to-parallel β-structure remodeling in Ac-AS occurs through helical/disordered species (Fig. 3). This finding correlates with previous works describing the population of helix-rich intermediates during AS aggregation under certain conditions [9,10]. Interestingly, the N-terminal region was shown to be especially sensitive to the formation of such intermediates [10], supporting our proposal on the key role of this portion of the protein in amyloid self-assembly. In line with this experimental observations,

in silico exploration of early oligomerization stages of the central amyloidogenic region of AS showed that dimers and trimers contain both α-helical and β-strand regions, the latter adopting a rich diversity of contacts but forming exclusively antiparallel β-sheets [65]. It is worth noting that helix-rich intermediates have been described in the aggregation pathway of other amyloidogenic proteins, such as the Aβ peptide of Alzheimer's disease and the islet amyloid polypeptide (IAPP) of type II diabetes, which has led to hypothesize that helical intermediates mediate early oligomerization of natively unstructured polypeptides and, therefore, they could be targets for anti-amyloid drugs [66]. We would like to highlight that the main structural signatures of the transient intermediates detected by time-dependent ATR-FTIR, *i.e.* antiparallel β-sheet structures combined with helical/disordered structures, are much alike those found for a variety of isolated kinetically trapped oAS [21–23] and are reminiscent of the compact, structured and highly toxic oAS identified by means of single-molecule FRET technique [3].

A structural mechanism for Aβ(1–40) peptide amyloid assembly has been recently proposed, in which a concerted 90° rotation in transiently populated Aβ oligomers formed by hydrophobic stacking of β-hairpins would form a fibril seed with in-register parallel β-sheets [67]. Based on the evidences discussed above, Ac-AS fibrillogenesis cannot just be explained by a reorientation of the strands by 90° since some of the early β-sheet interactions would need to be rearranged in another kind of secondary structure (helix/disordered) before fibril growth. Taking into account that the β4 region has high predicted β-sheet and aggregation propensities, is engaged in oligomeric intermolecular contacts [24], and lies towards the center of the fibril core [13], we postulate that this region remains structured as β-sheets during aggregation. Thus, a rotation around the longitudinal axis of β4 along with a restructuring of the most N-terminal β-regions would allow the remodeling of the β-sheet network to trigger fibril elongation. This hypothesis remains to be proven experimentally by, for instance, isotope-edited FTIR to provide a site-specific picture of such β-reorganization. Although this approach could not compete with NMR determinations in terms of atomic-scale resolution, the feasibility of such methodology to be applied at any stage of aggregation could provide fundamental knowledge on the local reorganization along fibrillogenesis [43].

As discussed above, amyloid formation is a complex process involving diverse intermediates varying in sizes, structures and morphologies. The complexity of such process can be rationalized within the framework provided by the energy landscape theory of protein folding/aggregation. In analogy to protein folding where a multitude of conformations is "funneled down" the native conformational ensemble *via* intramolecular interactions, intermolecular contacts lead the polypeptide chain to self-assembled states ending into formation of highly stable amyloid supramolecular aggregates [68]. Fig. 4 schematically depicts various aspects of α-synuclein conformational selection along amyloidogenesis discussed above. The native state of the protein is an ensemble of dynamically interchanging disordered conformers that transiently populate all the favored regions of the Ramachandran plot, including alpha, beta and PPII regions [50–52]. These dynamic secondary structures along with long-range tertiary interactions involving regions that lie outside the fibril core [15,16], modulate the fibrillation kinetics. Favored aggregation-prone conformations direct the disordered ensemble towards the bottom of the amyloid funnel. The rough energy landscape of protein aggregation and the multiplicity of assembly pathways lead to the possibility that distinguishable metastable oligomers can be kinetically trapped in local energy minima. This has an immediate biological impact since it might result that protein misfolding and aggregation in the cell can generate multiple species varying in sizes, secondary, tertiary and quaternary structures, and more importantly, different pathological roles. Thus, for instance, disordered intermediates exposing flexible hydrophobic surfaces can be engaged in widespread aberrant interactions with metastable proteins, antiparallel β-sheet oligomers could act as potent toxins by altering ion homeostasis, helical intermediates could promote fibril formation by increasing the local concentration of amyloidogenic sequences, and so forth. Besides, since the exact shape of the aggregation funnel depends on the environmental conditions, the balance among the different conformational states can be dynamically changed depending on the physiological/pathological scenarios.

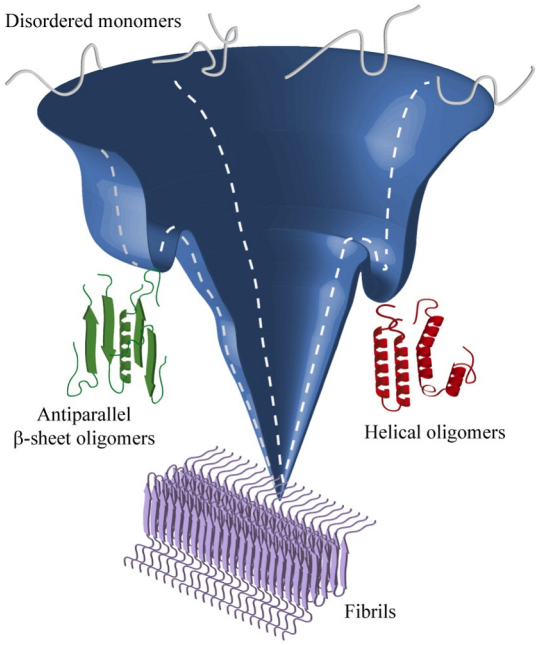

Fig. 4. Schematic energy landscape for amyloid aggregation of α-synuclein. The ensemble of natively disordered monomers lies on the top of the funnel, exhibiting high conformational entropy and transient tertiary contacts [16]. The surface "funnels" this multitude of conformations towards the formation of amyloid fibrils *via* intermolecular contacts. Such a surface, highly simplified in the scheme, resembles a rough funnel riddle with multiple local minima where distinct aggregation intermediates can be kinetically trapped. There is not a unique aggregation route but a multiplicity of aggregation pathways. Three representative trajectories for amyloid formation are shown as dash lines. Two (out of other possible) distinct intermediate species differing in secondary structure transiently populated along different pathways are schematically illustrated: antiparallel β-sheet intermediates (this work) and helix-rich intermediates [10]. The fibrillar state, where five-stranded β-sheet monomers are packed in a parallel in-register fashion [13], is represented at the bottom of the free energy surface.

In this work we present evidence that one of such aggregation pathways involves the spatial reorientation of β-strands at the prefibrillar level, providing valuable structural insights into the complex conformational switches occurring along the course of amyloid formation of the *in vivo* N^{α}-acetylated form of AS.

Declaration of interest

The authors declare that they have no conflicts of interest.

Transparency document

The Transparency document associated with this article can be found, in the online version.

Acknowledgments

We thank Dr. D. Mulvihill (University of Kent, UK) for kindly providing the pNatB plasmid. J.I.G. is a PhD fellow and M.S.C. is a Research Associate from the National Scientific and Technical Research Council of Argentina (CONICET). Financial support was received from Agencia Nacional de Promoción Científica y Tecnológica (grant PICT 2013-2603), CONICET (grant PIP-2011-2013), Secretaria de Ciencia y Tecnología, Universidad Nacional de Córdoba (grant SECyT-UNC 2014-2015), and international cooperation grants from Ministerio de Ciencia,

Tecnología e Innovación Productiva, Argentina — Fonds de la Recherche Scientifique, Belgium (MINCyT-FNRS, grant BE/12/01) and CONICET-FNRS (year 2012, grant V4/325C). R.S. is Postdoctoral Researcher, and V.R. is Senior Research Associate at F.R.S.-FNRS (Belgium). V.R. acknowledges financial supports from the F.R.S.-FNRS (PDR grant #70214.12) and SAO-FRA (grant S#14025).

References

[1] H.A. Lashuel, C.R. Overk, A. Oueslati, E. Masliah, The many faces of alpha-synuclein: from structure and toxicity to therapeutic target, Nat. Rev. Neurosci. 14 (2013) 38–48.
[2] H.L. Roberts, D.R. Brown, Seeking a mechanism for the toxicity of oligomeric alpha-synuclein, Biomolecules 5 (2015) 282–305.
[3] N. Cremades, S.I. Cohen, E. Deas, A.Y. Abramov, A.Y. Chen, A. Orte, M. Sandal, R.W. Clarke, P. Dunne, F.A. Aprile, C.W. Bertoncini, N.W. Wood, T.P. Knowles, C.M. Dobson, D. Klenerman, Direct observation of the interconversion of normal and toxic forms of alpha-synuclein, Cell 149 (2012) 1048–1059.
[4] G. Taschenberger, M. Garrido, Y. Tereshchenko, M. Bahr, M. Zweckstetter, S. Kugler, Aggregation of alphaSynuclein promotes progressive in vivo neurotoxicity in adult rat dopaminergic neurons, Acta Neuropathol. 123 (2012) 671–683.
[5] A.L. Mahul-Mellier, F. Vercruysse, B. Maco, N. Ait-Bouziad, M. De Roo, D. Muller, H.A. Lashuel, Fibril growth and seeding capacity play key roles in alpha-synuclein-mediated apoptotic cell death, Cell Death Differ. 22 (2015) 2107–2122.
[6] S.J. Wood, J. Wypych, S. Steavenson, J.C. Louis, M. Citron, A.L. Biere, alpha-Synuclein fibrillogenesis is nucleation-dependent. Implications for the pathogenesis of Parkinson's disease, J. Biol. Chem. 274 (1999) 19509–19512.
[7] V.N. Uversky, J. Li, A.L. Fink, Evidence for a partially folded intermediate in alpha-synuclein fibril formation, J. Biol. Chem. 276 (2001) 10737–10744.
[8] J. Kaylor, N. Bodner, S. Edridge, G. Yamin, D.P. Hong, A.L. Fink, Characterization of oligomeric intermediates in alpha-synuclein fibrillation: FRET studies of Y125W/Y133F/Y136F alpha-synuclein, J. Mol. Biol. 353 (2005) 357–372.
[9] M.M. Apetri, N.C. Maiti, M.G. Zagorski, P.R. Carey, V.E. Anderson, Secondary structure of α-synuclein oligomers: characterization by raman and atomic force microscopy, J. Mol. Biol. 355 (2006) 63–71.
[10] D. Ghosh, P.K. Singh, S. Sahay, N.N. Jha, R.S. Jacob, S. Sen, A. Kumar, R. Riek, S.K. Maji, Structure based aggregation studies reveal the presence of helix-rich intermediate during alpha-synuclein aggregation, Sci. Rep. 5 (2015) 9228.
[11] J.A. Fauerbach, D.A. Yushchenko, S.H. Shahmoradian, W. Chiu, T.M. Jovin, E.A. Jares-Erijman, Supramolecular non-amyloid intermediates in the early stages of alpha-synuclein aggregation, Biophys. J. 102 (2012) 1127–1136.
[12] H. Heise, W. Hoyer, S. Becker, O.C. Andronesi, D. Riedel, M. Baldus, Molecular-level secondary structure, polymorphism, and dynamics of full-length α-synuclein fibrils studied by solid-state NMR, Proc. Natl. Acad. Sci. U. S. A. 102 (2005) 15871–15876.
[13] M. Vilar, H.T. Chou, T. Luhrs, S.K. Maji, D. Riek-Loher, R. Verel, G. Manning, H. Stahlberg, R. Riek, The fold of α-synuclein fibrils, Proc. Natl. Acad. Sci. U. S. A. 105 (2008) 8637–8642.
[14] D. Eliezer, E. Kutluay, R. Bussell Jr., G. Browne, Conformational properties of alpha-synuclein in its free and lipid-associated states, J. Mol. Biol. 307 (2001) 1061–1073.
[15] C.W. Bertoncini, Y.S. Jung, C.O. Fernandez, W. Hoyer, C. Griesinger, T.M. Jovin, M. Zweckstetter, Release of long-range tertiary interactions potentiates aggregation of natively unstructured α-synuclein, Proc. Natl. Acad. Sci. U. S. A. 102 (2005) 1430–1435.
[16] S. Esteban-Martin, J. Silvestre-Ryan, C.W. Bertoncini, X. Salvatella, Identification of fibril-like tertiary contacts in soluble monomeric alpha-synuclein, Biophys. J. 105 (2013) 1192–1198.
[17] L. Breydo, V.N. Uversky, Structural, morphological, and functional diversity of amyloid oligomers, FEBS Lett. 589 (2015) 2640–2648.
[18] B.D. van Rooijen, K.A. van Leijenhorst-Groener, M.M. Claessens, V. Subramaniam, Tryptophan fluorescence reveals structural features of alpha-synuclein oligomers, J. Mol. Biol. 394 (2009) 826–833.
[19] S. Mysling, C. Betzer, P.H. Jensen, T.J. Jorgensen, Characterizing the dynamics of alpha-synuclein oligomers using hydrogen/deuterium exchange monitored by mass spectrometry, Biochemistry 52 (2013) 9097–9103.
[20] H.Y. Kim, M.K. Cho, A. Kumar, E. Maier, C. Siebenhaar, S. Becker, C.O. Fernandez, H.A. Lashuel, R. Benz, A. Lange, M. Zweckstetter, Structural properties of pore-forming oligomers of alpha-synuclein, J. Am. Chem. Soc. 131 (2009) 17482–17489.
[21] M.S. Celej, R. Sarroukh, E. Goormaghtigh, G.D. Fidelio, J.M. Ruysschaert, V. Raussens, Toxic prefibrillar alpha-synuclein amyloid oligomers adopt a distinctive antiparallel beta-sheet structure, Biochem. J. 443 (2012) 719–726.
[22] N. Lorenzen, S.B. Nielsen, A.K. Buell, J.D. Kaspersen, P. Arosio, B.S. Vad, W. Paslawski, G. Christiansen, Z. Valnickova-Hansen, M. Andreasen, J.J. Enghild, J.S. Pedersen, C.M. Dobson, T.P. Knowles, D.E. Otzen, The role of stable alpha-synuclein oligomers in the molecular events underlying amyloid formation, J. Am. Chem. Soc. 136 (2014) 3859–3868.
[23] S.W. Chen, S. Drakulic, E. Deas, M. Ouberai, F.A. Aprile, R. Arranz, S. Ness, C. Roodveldt, T. Guilliams, E.J. De-Genst, D. Klenerman, N.W. Wood, T.P. Knowles, C. Alfonso, G. Rivas, A.Y. Abramov, J.M. Valpuesta, C.M. Dobson, N. Cremades, Structural characterization of toxic oligomers that are kinetically trapped during alpha-synuclein fibril formation, Proc. Natl. Acad. Sci. U. S. A. 112 (2015) E1994–E2003.
[24] J.I. Gallea, M.S. Celej, Structural insights into amyloid oligomers of the Parkinson disease-related protein alpha-synuclein, J. Biol. Chem. 289 (2014) 26733–26742.
[25] J.P. Anderson, D.E. Walker, J.M. Goldstein, R. de Laat, K. Banducci, R.J. Caccavello, R. Barbour, J. Huang, K. Kling, M. Lee, L. Diep, P.S. Keim, X. Shen, T. Chataway, M.G. Schlossmacher, P. Seubert, D. Schenk, S. Sinha, W.P. Gai, T.J. Chilcote, Phosphorylation of Ser-129 is the dominant pathological modification of alpha-synuclein in familial and sporadic Lewy body disease, J. Biol. Chem. 281 (2006) 29739–29752.
[26] B. Fauvet, M.B. Fares, F. Samuel, I. Dikiy, A. Tandon, D. Eliezer, H.A. Lashuel, Characterization of semisynthetic and naturally Nalpha-acetylated alpha-synuclein in vitro and in intact cells: implications for aggregation and cellular properties of alpha-synuclein, J. Biol. Chem. 287 (2012) 28243–28262.
[27] A.S. Maltsev, J. Ying, A. Bax, Impact of N-terminal acetylation of alpha-synuclein on its random coil and lipid binding properties, Biochemistry 51 (2012) 5004–5013.
[28] L. Kang, G.M. Moriarty, L.A. Woods, A.E. Ashcroft, S.E. Radford, J. Baum, N-terminal acetylation of alpha-synuclein induces increased transient helical propensity and decreased aggregation rates in the intrinsically disordered monomer, Protein Sci. 21 (2012) 911–917.
[29] L. Kang, M.K. Janowska, G.M. Moriarty, J. Baum, Mechanistic insight into the relationship between N-terminal acetylation of alpha-synuclein and fibril formation rates by NMR and fluorescence, PLoS One 8 (2013), e75018.
[30] M. Johnson, A.T. Coulton, M.A. Geeves, D.P. Mulvihill, Targeted amino-terminal acetylation of recombinant proteins in *E. coli*, PLoS One 5 (2010), e15801.
[31] M.S. Celej, E.A. Jares-Erijman, T.M. Jovin, Fluorescent N-arylaminonaphthalene sulfonate probes for amyloid aggregation of α-synuclein, Biophys. J. 94 (2008) 4867–4879.
[32] Y.N. Chirgadze, N.A. Nevskaya, Infrared spectra and resonance interaction of amide-I vibration of the antiparallel-chain pleated sheet, Biopolymers 15 (1976) 607–625.
[33] D.M. Byler, H. Susi, Examination of the secondary structure of proteins by deconvolved FTIR spectra, Biopolymers 25 (1986) 469–487.
[34] E. Goormaghtigh, V. Cabiaux, J.M. Ruysschaert, Determination of soluble and membrane protein structure by Fourier transform infrared spectroscopy. III. Secondary structures, Subcell. Biochem. 23 (1994) 405–450.
[35] E. Goormaghtigh, V. Cabiaux, J.M. Ruysschaert, Determination of soluble and membrane protein structure by Fourier transform infrared spectroscopy. I. Assignments and model compounds, Subcell. Biochem. 23 (1994) 329–362.
[36] A. Barth, C. Zscherp, What vibrations tell us about proteins, Q. Rev. Biophys. 35 (2002) 369–430.
[37] M.J. Hope, M.B. Bally, G. Webb, P.R. Cullis, Production of large unilamellar vesicles by a rapid extrusion procedure: characterization of size distribution, trapped volume and ability to maintain a membrane potential, Biochim. Biophys. Acta 812 (1985) 55–65.
[38] G.R. Bartlett, Phosphorus assay in column chromatography, J. Biol. Chem. 234 (1959) 466–468.
[39] A. Gustot, J.I. Gallea, R. Sarroukh, M.S. Celej, J.M. Ruysschaert, V. Raussens, Amyloid fibrils are the molecular trigger of inflammation in Parkinson's disease, Biochem. J. 471 (2015) 323–333.
[40] C.W. Bertoncini, M.S. Celej, Small molecule fluorescent probes for the detection of amyloid self-assembly in vitro and in vivo, Curr. Protein Pept. Sci. 12 (2011) 205–220.
[41] B.D. van Rooijen, M.M. Claessens, V. Subramaniam, Lipid bilayer disruption by oligomeric alpha-synuclein depends on bilayer charge and accessibility of the hydrophobic core, Biochim. Biophys. Acta 1788 (2009) 1271–1278.
[42] G. Zandomeneghi, M.R. Krebs, M.G. McCammon, M. Fandrich, FTIR reveals structural differences between native beta-sheet proteins and amyloid fibrils, Protein Sci. 13 (2004) 3314–3321.
[43] R. Sarroukh, E. Goormaghtigh, J.M. Ruysschaert, V. Raussens, ATR-FTIR: a "rejuvenated" tool to investigate amyloid proteins, Biochim. Biophys. Acta 1828 (2013) 2328–2338.
[44] Y.N. Chirgadze, N.A. Nevskaya, Infrared spectra and resonance interaction of amide-I vibration of the paraellel-chain pleated sheets, Biopolymers 15 (1976) 627–636.
[45] Y.A. Lazarev, B.A. Grishkovsky, T.B. Khromova, Amide I band of IR spectrum and structure of collagen and related polypeptides, Biopolymers 24 (1985) 1449–1478.
[46] A.R. Viguera, J.L. Arrondo, A. Musacchio, M. Saraste, L. Serrano, Characterization of the interaction of natural proline-rich peptides with five different SH3 domains, Biochemistry 33 (1994) 10925–10933.
[47] C.D. Syme, E.W. Blanch, C. Holt, R. Jakes, M. Goedert, L. Hecht, L.D. Barron, A Raman optical activity study of rheomorphism in caseins, synucleins and tau. New insight into the structure and behaviour of natively unfolded proteins, Eur. J. Biochem. 269 (2002) 148–156.
[48] N.C. Maiti, M.M. Apetri, M.G. Zagorski, P.R. Carey, V.E. Anderson, Raman spectroscopic characterization of secondary structure in natively unfolded proteins: alpha-synuclein, J. Am. Chem. Soc. 126 (2004) 2399–2408.
[49] V.L. Anderson, W.W. Webb, D. Eliezer, Interplay between desolvation and secondary structure in mediating cosolvent and temperature induced alpha-synuclein aggregation, Phys. Biol. 9 (2012) 056005.
[50] C. Camilloni, A. De Simone, W.F. Vranken, M. Vendruscolo, Determination of secondary structure populations in disordered states of proteins using nuclear magnetic resonance chemical shifts, Biochemistry 51 (2012) 2224–2231.
[51] J. Roche, J. Ying, A.S. Maltsev, A. Bax, Impact of hydrostatic pressure on an intrinsically disordered protein: a high-pressure NMR study of alpha-synuclein, Chembiochem 14 (2013) 1754–1761.
[52] M. Schwalbe, V. Ozenne, S. Bibow, M. Jaremko, L. Jaremko, M. Gajda, M.R. Jensen, J. Biernat, S. Becker, E. Mandelkow, M. Zweckstetter, M. Blackledge, Predictive atomic resolution descriptions of intrinsically disordered hTau40 and alpha-synuclein in solution from NMR and small angle scattering, Structure 22 (2014) 238–249.
[53] B.D. van Rooijen, M.M. Claessens, V. Subramaniam, Membrane binding of oligomeric alpha-synuclein depends on bilayer charge and packing, FEBS Lett. 582 (2008) 3788–3792.
[54] F. Chiti, C.M. Dobson, Protein misfolding, functional amyloid, and human disease, Annu. Rev. Biochem. 75 (2006) 333–366.

[55] M. Chen, M. Margittai, J. Chen, R. Langen, Investigation of α-synuclein fibril structure by site-directed spin labeling, J. Biol. Chem. 282 (2007) 24970–24979.
[56] P. Zabrocki, I. Bastiaens, C. Delay, T. Bammens, R. Ghillebert, K. Pellens, C. De Virgilio, F. Van Leuven, J. Winderickx, Phosphorylation, lipid raft interaction and traffic of alpha-synuclein in a yeast model for Parkinson, Biochim. Biophys. Acta 1783 (2008) 1767–1780.
[57] A. Varshavsky, The N-end rule pathway and regulation by proteolysis, Protein Sci. 20 (2011) 1298–1345.
[58] W.S. Davidson, A. Jonas, D.F. Clayton, J.M. George, Stabilization of alpha-synuclein secondary structure upon binding to synthetic membranes, J. Biol. Chem. 273 (1998) 9443–9449.
[59] E. Cerf, R. Sarroukh, S. Tamamizu-Kato, L. Breydo, S. Derclaye, Y.F. Dufrene, V. Narayanaswami, E. Goormaghtigh, J.M. Ruysschaert, V. Raussens, Antiparallel beta-sheet: a signature structure of the oligomeric amyloid beta-peptide, Biochem. J. 421 (2009) 415–423.
[60] R. Sarroukh, E. Cerf, S. Derclaye, Y.F. Dufrene, E. Goormaghtigh, J.M. Ruysschaert, V. Raussens, Transformation of amyloid beta(1–40) oligomers into fibrils is characterized by a major change in secondary structure, Cell. Mol. Life Sci. 68 (2011) 1429–1438.
[61] A. Natalello, V.V. Prokorov, F. Tagliavini, M. Morbin, G. Forloni, M. Beeg, C. Manzoni, L. Colombo, M. Gobbi, M. Salmona, S.M. Doglia, Conformational plasticity of the Gerstmann–Straussler–Scheinker disease peptide as indicated by its multiple aggregation pathways, J. Mol. Biol. 381 (2008) 1349–1361.
[62] H. Fabian, K. Gast, M. Laue, R. Misselwitz, B. Uchanska-Ziegler, A. Ziegler, D. Naumann, Early stages of misfolding and association of beta2-microglobulin: insights from infrared spectroscopy and dynamic light scattering, Biochemistry 47 (2008) 6895–6906.
[63] Y. Zou, Y. Li, W. Hao, X. Hu, G. Ma, Parallel beta-sheet fibril and antiparallel beta-sheet oligomer: new insights into amyloid formation of hen egg white lysozyme under heat and acidic condition from FTIR spectroscopy, J. Phys. Chem. B 117 (2013) 4003–4013.
[64] F.S. Ruggeri, G. Longo, S. Faggiano, E. Lipiec, A. Pastore, G. Dietler, Infrared nanospectroscopy characterization of oligomeric and fibrillar aggregates during amyloid formation, Nat. Commun. 6 (2015) 7831.
[65] C. Eugene, R. Laghaei, N. Mousseau, Early oligomerization stages for the non-amyloid component of alpha-synuclein amyloid, J. Chem. Phys. 141 (2014) 135103.
[66] A. Abedini, D.P. Raleigh, A role for helical intermediates in amyloid formation by natively unfolded polypeptides? Phys. Biol. 6 (2009) 015005.
[67] W. Hoyer, C. Gronwall, A. Jonsson, S. Stahl, T. Hard, Stabilization of a beta-hairpin in monomeric Alzheimer's amyloid-beta peptide inhibits amyloid formation, Proc. Natl. Acad. Sci. U. S. A. 105 (2008) 5099–5104.
[68] B. Ma, R. Nussinov, Selective molecular recognition in amyloid growth and transmission and cross-species barriers, J. Mol. Biol. 421 (2012) 172–184.